ORIGINAL PAPER

Georg M. Partzsch · Dominique Lattard
Catherine McCammon

Mössbauer spectroscopic determination of Fe^{3+}/Fe^{2+} in synthetic basaltic glass: a test of empirical fO_2 equations under superliquidus and subliquidus conditions

Abstract One of the most widely used methods to estimate magmatic oxygen fugacity involves the use of empirical equations relating fO_2 to the iron redox state in quenched silicate liquids; however none of the equations have been calibrated experimentally under subliquidus conditions at temperatures and oxygen fugacities that are relevant to natural magmas. To address this problem, we tested two empirical relationships [Eq. (1) in Kress and Carmichael 1991; Eq. (6) in Nikolaev et al. 1996] on synthetic glasses synthesized from a ferrobasaltic and a transitional alkali-basaltic composition at sub- to superliquidus temperatures (1,132–1,222°C) and controlled oxygen fugacities ($\Delta FMQ = -2$ to $+1.4$). $Fe^{3+}/\Sigma Fe$ was determined using conventional and milliprobe Mössbauer spectroscopy, and verified using wet chemical analysis on selected samples. For the ferrobasaltic bulk composition "SC1-P", both empirical models reproduce the $Fe^{3+}/\Sigma Fe$ ratio of the quenched liquids generally within 0.03 for sub- as well as superliquidus temperatures, although agreement is worse at higher oxygen fugacities ($\Delta FMQ > +1$) at subliquidus temperatures. For the transitional alkali-basaltic composition "7159V-P", both models reproduce the $Fe^{3+}/\Sigma Fe$ ratio of the quenched liquids generally within 0.04, although agreement is worse for both models at high oxygen fugacities ($\Delta FMQ > +1$). Such behaviour may be related to a change in melt structure, where a progressive change in Fe^{3+} coordination is inferred to occur as a function of $Fe^{3+}/\Sigma Fe$ based on Mössbauer center shifts. Recasting the data in terms of oxygen fugacity shows that calculated oxygen fugacities deviate from those actually maintained during the equilibration of the sample material by generally no more than 0.5 log-bar unit, with maximum deviations that only rarely exceed one log-bar unit.

G. M. Partzsch (✉) · D. Lattard
Mineralogisches Institut, Universität Heidelberg,
INF 236, 69120 Heidelberg, Germany
E-mail: partzsch@min.uni-heidelberg.de
Tel.: +49-6221-546023
Fax: +49-6221-544805

C. McCammon
Bayerisches Geoinstitut, Universität Bayreuth,
95440 Bayreuth, Germany

Introduction

There is a continuing interest in determining the oxygen fugacity (fO_2) prevailing in basic magmas, because fO_2 exerts a major control on the redox state of iron (Fe^{3+}/Fe^{2+}) in the liquid (e.g. Kennedy 1948; Sack et al. 1980). The iron redox state influences, in turn, the rheology and density of the liquid (e.g. Dingwell and Virgo 1987; Virgo 1987; Dingwell and Brearley 1988), and partly determines the crystallization sequence and the composition of precipitating minerals (e.g. Snyder et al. 1993; Toplis and Carroll 1995). On the whole, fO_2 plays a dominant role during magmatic crystallization-differentiation processes and its knowledge is necessary to model these processes and to retrieve liquid lines of descent.

Several methods have been employed to estimate the oxygen fugacity in magmas, but the most widely used rely on empirical equations relating fO_2 to the iron redox state in quenched silicate liquids. These equations were calibrated on the basis of superliquidus experiments (1,200–1,640° C) performed under known fO_2 (Fig. 1) on a wide variety of volcanic rocks (e.g. Sack et al. 1980). After quenching the glassy samples were analyzed, primarily using the electron microprobe, to determine the concentrations of all major oxides (incl. FeO_{tot}), but also utilizing a wet chemical method to retrieve the FeO contents. The Fe_2O_3 contents were subsequently calculated by difference, where

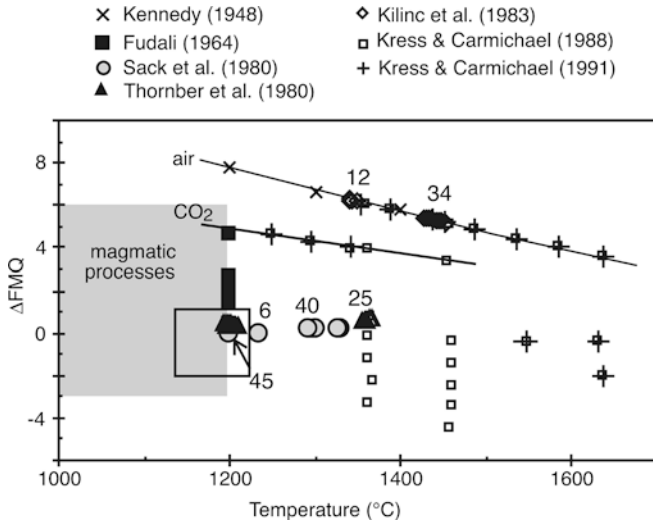$$Fe_2O_3(wt\%) = (FeO_{tot} - FeO)\frac{159.6922}{2 * 71.8464}.$$

Fig. 1 Temperature and oxygen fugacities (ΔFMQ) of the experiments used to calibrate the empirical equations relating f_{O_2} to the iron redox state in quenched silicate liquids. The numbers of experiments performed in the same T-f_{O_2} conditions are written above the corresponding symbols. The *shaded area* indicates typical conditions for natural magmatic processes, while the *unshaded rectangle* shows the conditions of our experiments. ΔFMQ = log f_{O_2} (experimental) − log f_{O_2} (FMQ buffer) with FMQ values after O'Neill (1987)

A critical review of previous work

Sack et al. (1980) established the first formulation of an equation relating the iron redox ratio to the oxygen fugacity, the temperature and the bulk composition for complex natural silicate liquids quenched to glasses:

$$\ln\left(X_{Fe_2O_3}^{liq}/X_{FeO}^{liq}\right) = a\ln f_{O_2} + \frac{b}{T} + c + \sum_i d_i X_i \qquad (1)$$

where T is the temperature in Kelvin, X_i the mole fractions of SiO_2, Al_2O_3, FeO_{tot}, MgO, CaO, Na_2O, K_2O and $X_{Fe_2O_3}^{liq}$, X_{FeO}^{liq} the mole fractions of FeO and Fe_2O_3 in the liquid/glass. The constants a, b, c and d_i were determined by regression analysis on a data set involving 143 samples. This set included not only the results of 57 new experiments performed at f_{O_2} around those of the FMQ buffer (fayalite-magnetite-quartz) on molten volcanic rocks with compositions spanning virtually the entire known range, but also comprised superliquidus experiments on basic compositions performed either in air (i.e. at ΔFMQ +5 to +8; Kennedy 1948) or in the range ΔFMQ 0 to +8 (Fudali 1965; Shibata 1967; Thornber et al. 1980; Fig. 1).

Kilinc et al. (1983) added 46 new melting experiments at 1,350–1,450°C in air (Fig. 1). On the basis of a total of 186 calibration experiments, they refined the regression coefficients of Eq. (1) to new values with standard errors reduced to about a third of those determined by Sack et al. (1980).

Kress and Carmichael (1988) expanded the calibration range to higher temperatures (up to 1,636°C) and

lower f_{O_2} (down to ΔFMQ −3.5; Fig. 1) and combined these results with the data set used by Kilinc et al. (1983) to estimate thermodynamic parameters for the following iron redox reaction in natural melts:

$$FeO + 0.232\, O_2 = Fe_{O_{1.464}}$$
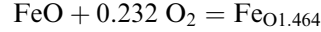
The authors found that the data could be well accounted for by a model based on simple mixing between FeO and a completely associated $FeO_{1.464}$ component. Consequently they formulated a new empirical equation:

$$\ln\left(X_{FeO_{1.464}}^{liq}/X_{FeO}^{liq}\right) = 0.232\ \ln f_{O_2} - \frac{\Delta H_r}{RT} + \frac{\Delta S_r}{R}$$
$$- \frac{1}{RT}\sum_i \Delta W_i X_i \qquad (2)$$

where ΔH_r and ΔS_r are the enthalpy and entropy of the iron oxidation reaction given above and W_i the Margules mixing terms.

In a subsequent paper, Kress and Carmichael (1991) corrected some of their previous analytical results, quantified the compressibility of silicate liquids via measurements of the ultrasonic acoustic velocities in air, abandoned their thermodynamically based equation [Eq. (2)] and proposed a revised and expanded version:

$$\ln\left(X_{Fe_2O_3}^{liq}/X_{FeO}^{liq}\right) = a\ln f_{O_2} + \frac{b}{T} + c$$
$$+ \sum_i d_i X_i + e\left[1 - \frac{T_o}{T} - \ln\left(\frac{T}{T_o}\right)\right]$$
$$+ f\frac{P}{T} + g\frac{(T - T_o)P}{T} + h\frac{P^2}{T}$$
$$\qquad (3)$$

where T_o is the reference temperature (1,673 K) and P the pressure (in Pa). The values for a, b, c, and d_i were estimated through a weighted step-wise linear regression of the results of 228 individual experiments from Kennedy (1948), Fudali (1965), Thornber et al. (1980), Sack et al. (1980), Kilinc et al. (1983), Kress and Carmichael (1988) and Kress and Carmichael (1991). The value for e stemmed from Stebbins et al. (1984), and those for f, g, and h were refined using the results of the ultrasonic experiments. The last four terms of the equation, i.e. those with the e, f, g and h coefficients, have negligible values at temperatures beneath 1,600°C and pressures beneath 1 GPa. In this P-T-range Eq. (3) is practically reduced to Eq. (1). However, in contrast to Sack et al. (1980), neither Kilinc et al. (1983) nor Kress and Carmichael (1991) found a dependence of the iron redox ratio from the SiO_2 and MgO contents of the quenched melts and dismissed the corresponding regression coefficients (d_{SiO2}, d_{MgO}).

In the course of a comprehensive study of the relations between structure and redox equilibria in simple synthetic systems as well as in complex magmatic liquids, Mysen (1987, 1991) proposed a new expression with structural rather than oxide components:

$$\ln\left(\frac{Fe^{2+}}{Fe^{3+}}\right) = a + \frac{b}{T} + c\ln f_{O_2} + d\frac{Al}{Al + Si}$$
$$+ e\frac{Fe^{3+}}{Fe^{3+} + Si} + \sum_{j=i}^{j} f_j(NBO/T)_j \qquad (4)$$

where NBO/T is the ratio of nonbridging oxygens to tetrahedrally coordinated cations (expressing the degree of polymerization of the melt) and f_j the regression coefficients for the individual network-modifying oxides. The constants a, b, c and d were, together with f_j, obtained from stepwise, linear regression, using a combination of the data bases of Sack et al. (1980) and Kilinc et al. (1983) as well as 267 analyses from glasses in simple synthetic systems (Seifert et al. 1979; Virgo et al. 1981; Mysen and Virgo 1983; Virgo and Mysen 1985; Mysen et al. 1980, 1984, 1985a, b).

In the mean time, Borisov (1988) pointed out that the values of the constant b in Eqs. (1) to (4) may vary greatly, apparently in relation to the bulk chemistry of the quenched melts. As a consequence, Borisov and Shapkin (1990) came up with an equation in which all constants were completed by expressions dependent on the bulk composition:

$$\ln\left(\frac{FeO_{1.5}}{FeO}\right) = \left(a + \sum d_i'' X_i\right)\log f_{O_2}$$
$$+ \left(b + \sum d_i' X_i\right)\frac{1}{T} + c + \sum d_i X_i. \qquad (5)$$

Nikolaev et al. (1996) tested the six equations already proposed (1a: Sack et al. 1980; 1b: Kilinc et al. 1983; 2: Kress and Carmichael 1988; 3: Kress and Carmichael 1991; 4: Mysen 1987, 1991; 5: Borisov and Shapkin 1990) on a choice of 170 of the experimental results on natural liquids previously reported. They did not consider the runs under oxidizing conditions ($\Delta FMQ > +1.7$) and chose to distribute the samples into four separate series (tholeiitic, subalkaline, alkaline and andesite-rhyolite series) according to their bulk SiO_2 and $(Na_2O + K_2O)$ contents. Nikolaev et al. (1996) found that for the first three series, all six equations estimate the ferric-ferrous ratio with comparable average accuracy. The average deviation between the experimental and calculated values of $\log(Fe^{3+}/Fe^{2+})$ is around 0.04. Nevertheless, Nikolaev et al. (1996) proposed for these first three series three new sets of regression coefficients for the following equation:

$$\log\left(Fe^{3+}/Fe^{2+}\right)_{liq} = a\log f_{O_2} + \frac{b}{T} + \sum_i d_i X_i. \qquad (6)$$

The authors did not consider the andesite-rhyolite series further because all equations failed to reproduce the Fe^{3+}/Fe^{2+} values in the case of two or three acidic melts from this series. However, it is apparent from Fig. 2 of Nikolaev et al. (1996) that the agreement between experimental and calculated values for other samples of the andesite-rhyolite series is similar to

agreement for the other series. In view of the results presented by Nikolaev et al. (1996) in their Table 4 and Fig. 3, their new equation for the tholeiitic series apparently improves the Fe^{3+}/Fe^{2+} estimates, particularly at low f_{O_2}.

The most frequently used versions of the equation relating iron redox ratio and oxygen fugacity in natural quenched silicate melts are those of Sack et al. (1980), Kilinc et al. (1983) and the simplified equation of Kress and Carmichael (1991), i.e. in all cases form (1) of the equation. Formulation (2) was not further applied, even by the authors themselves and the expressions proposed by the Russian groups (5 and 6) did not reach a large audience. The equations of type (1) were utilized to estimate the oxygen fugacity in volcanic rocks of known bulk ferric-ferrous ratio (e.g. Luhr and Carmichael 1985; Wallace and Carmichael 1992, 1994) or to retrieve Fe^{3+}/Fe^{2+} values in glasses present in run products equilibrated at known temperature and fO_2 (e.g. Snyder et al. 1993; Thy and Lofgren 1994; Toplis and Carroll 1995). Equation (4) of Mysen (1987, 1991) can be used only to retrieve the oxygen fugacity if structural information on the melt/glass structure is available, in particular concerning the coordination of Fe^{3+}.

Aim of the present study

In relation to an experimental study on the crystallization-differentiation of ferrobasaltic magmas under conditions closed to oxygen (Lattard and Partzsch 2001), we are especially interested in retrieving accurate oxygen fugacity values from the ferric-ferrous ratios of melts coexisting with crystals under subliquidus conditions, at temperatures below 1,200°C and at moderate to reduced fO_2 conditions. The question arises whether the equations discussed above may be used, because the relevant conditions are outside the calibration range of the equations, both with respect to temperature and to oxygen fugacity (Fig. 1). In fact, this question applies to many past or present studies because the calibration range of the equations is not that of natural magmatic rocks (Fig. 1). The calibration temperatures are typically very high in order to ensure complete melting of the samples. Moreover, as already pointed out by Ariskin and Barmina (1999), highly oxidizing conditions are over-represented in the databases. Therefore, there is a clear need for new experimental data on the ferric-ferrous ratio of quenched melts under subliquidus conditions and moderate to low fO_2, i.e. under conditions relevant for processes in magma chambers.

The present study was planned to determine Fe^{3+}/Fe^{2+} values from quenched melt pockets between crystals with the help of a Mössbauer milliprobe, which allows measurements on glass samples as small as 50 µm in diameter. The samples were obtained from crystalli-

zation experiments on a ferrobasaltic composition in the temperature range 1,130–1,180°C, under redox conditions between $\Delta FMQ-2$ and $\Delta FMQ+1.4$. To compare the ferric-ferrous ratios retrieved from the Mössbauer spectra with those obtained by combining wet chemical and microprobe analyses, we also prepared a set of glassy samples at superliquidus temperatures to be analyzed by both methods. To check the effect of bulk composition and temperature on the Fe^{3+}/Fe^{2+} values, the study was supplemented with a few superliquidus experiments (1,180–1,222°C) on both the ferrobasaltic and a transitional alkali-basaltic composition.

Finally, we have tested whether the two most recent calibrations of the equations discussed before, those of Kress and Carmichael (1991) and Nikolaev et al. (1996), are able to reproduce the $Fe^{3+}/\Sigma Fe$ values that we retrieved from Mössbauer spectroscopy on our synthetic glasses.

Experimental procedure

Starting materials

The starting materials were two synthetic eight-component glass powders synthesized from mixtures of oxides (SiO_2, TiO_2, Al_2O_3, Fe_2O_3, MgO) and carbonates ($CaCO_3$, Na_2CO_3 and K_2CO_3). The mixtures were decarbonated at 800°C in a Pt-crucible for 0.5 h, fused at 1,400°C in air for 5 h and poured for quenching into a steel mortar. The material was homogenized by repeated grinding and fusing.

The first starting material (SC1-P; Table 1) has a ferrobasaltic composition similar to that of a proposed parental magma for the exposed part of the Skaergaard Intrusion (Basaltic dyke C of Brooks and Nielsen 1978). The phase equilibria on this composition have been determined in detail as a function of temperature and oxygen fugacity by Toplis and Carroll (1995). The composition of the second glass (7159V-P; Table 1) is that of a transitional alkalic basalt similar to a lava from the 1973 Eldfell eruption on Heimaey, Iceland (Thy and Lofgren 1994). Both starting materials have relatively

high bulk iron contents (13 and 14.4 wt.% FeO_{tot}; Table 1), and their $Fe^{3+}/\Sigma Fe$ values are high because only Fe_2O_3 was used in the starting mixtures and the fusing occurred in air (i.e. at about $\Delta FMQ = +5$).

High-temperature experiments

Techniques

Charges of the starting materials were equilibrated at high temperatures and controlled oxygen fugacities. All experiments were performed at atmospheric pressure in a vertical drop-quench furnace (Gero) with gas mixing facilities to control fO_2. The samples were suspended in the hot spot (±0.5°C, approximately 3 cm in length) with furnace temperature controlled within 0.2°C by a commercial controller. At the end of the runs the samples were drop-quenched into distilled water. The temperature was measured before and after each experiment by a $Pt/Pt_{90}Rh_{10}$ thermocouple that had been calibrated against the melting points of Ag (960.8°C), Au (1,064.4°C) and Cu (1,083.5°C). The temperature uncertainty is estimated to be ±2°C. The oxygen fugacity was fixed by mixing high purity CO and CO_2 (Deines et al. 1974) with electronic mass flow controllers (Millipore). The oxygen fugacity was measured in the hot spot of the furnace using an yttrium-stabilized zirconia probe (with air as reference) that was calibrated against the Ni-NiO (O'Neill 1987) and magnetite-wüstite (O'Neill 1988) solid buffers. A conservative estimate of the uncertainties in log fO_2 values is ±0.2 log-bar units.

The sample holders were loops (diameter: 2–3 mm) of platinum wire (0.1 mm). Aliquots of 40–60 mg starting material were loaded onto the loops using polyvinyl alcohol as a binder according to the loop-technique (e.g. Presnall and Brenner 1974; Toplis and Carroll 1995). To minimize iron loss from the sample to the platinum wire (e.g. Johannes and Bode 1978; Ford 1978) the loops were "presaturated" with iron using one of the following methods. The loops used in most experiments were presaturated by heating them in contact with some starting material at 1,180°C under the required oxygen fugacities for 24 h, followed by cleaning in HF. For the last six experiments (OS 86 to OS 93; Table 2), Fe_2O_3 was used instead of the starting material for the presaturation procedure. Apart from the advantage of conserving the starting material, iron oxide proved much easier to remove from the loop.

Superliquidus experiments

Superliquidus experiments were conducted with both starting compositions at temperatures between 1,183°C and 1,222°C (Table 2). The liquidus of 7159V-P lies below 1,150°C, and that of SC1-P is between 1,179 and 1,183°C. To obtain enough sample for wet chemical

Table 1 Results of electron microprobe analyses (wt.%) of the starting materials (means and 1σ standard deviations over n single analyses)

	SC1-P		7159V-P	
n	33		29	
SiO_2	47.42	(15)	47.88	(20)
TiO_2	2.86	(6)	4.04	(10)
Al_2O_3	14.08	(12)	13.22	(16)
FeO_{tot}	12.97	(22)	14.38	(21)
MgO	6.32	(6)	3.23	(6)
CaO	10.73	(8)	9.04	(8)
Na_2O	2.80	(6)	4.68	(8)
K_2O	0.35	(2)	1.15	(4)
Total	97.53		97.62	

Table 2 Run conditions and results of wet chemical and Mössbauer spectroscopic determinations of $Fe^{3+}/\Sigma Fe$ in quenched glasses

Columns under *Glass composition*: Na_2O loss, FeO_{tot}, ΔFeO_{tot}. Columns reporting $Fe^{3+}/\Sigma Fe$[g]: EMP+ wet chem., C.Möss.[h], Möss.M.[i], Calc. K&C[j], Calc. N(I)[k], Calc. N(II)[l]. Values in parentheses are the number of determinations.

Starting material	Run no.[a]	T (°C)[b]	ΔFMQ[c]	t (h)	Phases[d]	Na_2O loss (% rel.)	FeO_{tot} (wt.%)[e]	ΔFeO_{tot}[f] (% rel.)	EMP+ wet chem.	C.Möss.[h]	Möss.M.[i]	Calc. K&C[j]	Calc. N(I)[k]	Calc. N(II)[l]
SC1-P Superliquidus (T > 1,180 °C)														
	OS77d	1,221	1.45	19.5	Gl	−1.8	12.90	−0.5			0.23 (5)	0.24	0.20	
	OS89	1,189	1.45	21	Gl	–	12.95	–	0.33 (5)			0.24	0.20	
	OS82	1,187	1.41	23.5	Gl	−1.4	12.77	−1.5			0.24 (4)	0.24	0.20	
	OS79d	1,222	0.10	19.5	Gl	−1.8	12.88	−0.7			0.16 (4)	0.15	0.14	
	OS87-R	1,189	0.02	20	Gl	−5.7	13.22	+1.9*			0.15 (4)	0.14	0.13	
	OS80	1,186	0.02	19	Gl	−2.5	12.87	−0.8			0.11 (4)	0.14	0.14	
	OS91	1,185	0.01	20	Gl	−1.1	13.26	+2.2*				0.14	0.14	
	OS85	1,188	−1.02	45.5	Gl	−6.1	12.37	−4.6	0.18 (5)		0.13 (4)	0.09	0.10	
	OS88-R	1,188	−1.02	20	Gl	–	13.30	+2.5*			0.11 (4)	0.09	0.10	
	OS90	1,185	−1.02	21	Gl	–	13.32	+2.7*	0.11 (5)			0.09	0.10	
	OS81d	1,221	−1.84	22	Gl	−2.5	12.99	–			0.09 (4)	0.07	0.08	
	OS93	1,189	−1.92	63	Gl	–	13.46	+3.8*			0.08 (4)	0.06	0.08	
	OS86	1,188	−1.88	20.5	Gl	–	13.19	+2.2*	0.08 (5)		0.08 (4)	0.07	0.08	
	OS84	1,185	−1.93	45	Gl	−6.8	11.97	−7.7			0.08 (4)	0.06	0.08	
	OS19	1,184	−1.97	23.5	Gl, Pl	−3.2	12.68	−2.2		0.11 (5)		0.06	0.07	
Subliquidus (1,132–1,174 °C)														
	OS8	1,172	1.31	40	Gl, Pl		13.61			0.29 (5)		0.23	0.20	
	OS10	*1,162*	1.29	46	Gl, Pl		13.04			0.25 (4)		0.22	0.21	
	OS1b	1,174	−0.02	90	Gl, Pl		12.44			0.13 (4)		0.14	0.13	
	OS3a	1,154	−0.05	67	Gl, Pl, Ol		13.67			0.16 (4)		0.14	0.14	
	OS18	*1,132*	−0.08	48	Gl, Pl, Ol		14.82			0.12 (3)		0.13	0.16	
	OS13	*1,149*	−1.17	67.25	Gl, Pl, Ol		13.48			0.12 (4)		0.09	0.10	
	OS17	*1,151*	−2.03	55	Gl, Pl, Ol		13.94			0.07 (4)		0.06	0.08	
	OS21	*1,132*	−2.09	76	Gl, Pl, Ol		14.94			0.11 (5)		0.06	0.09	
7159V-P Superliquidus (1,183–1,222 °C)														
	OS77a	1,221	1.45	19.5	Gl	–	13.88	3.9			0.40 (6)	0.25	0.21	0.30
	OS68a	1,183	0.84	8	Gl	–	14.28	0.8			0.30 (5)	0.21	0.13	0.25
	OS79a	1,222	0.10	19.5	Gl	–	14.02	2.8			0.14 (4)	0.16	0.14	0.20
	OS78a	1,221	−0.94	18.5	Gl	−2.8	14.18	1.5			0.14 (4)	0.10	0.16	0.14
	OS70a	1,183	−1.00	8	Gl	−2.6	14.15	1.8			0.12 (4)	0.10	0.10	0.13
	OS81a	1,221	−1.84	22	Gl	−6.8	14.13	1.9			0.12 (4)	0.07	0.09	0.07

[a] –R: reversal experiments; [b] *italics*: final temperature attained after a temperature ramp (See details in section "Experimental procedure"); [c] $\Delta FMQ = \log fO_2(\text{experiment}) - \log fO_2(\text{FMQ}$ buffer) (O'Neill 1987); [d] abbreviations for the phases present in the run products: Gl: glass; Pl: plagioclase; Ol: olivine; [e] total FeO from electron microprobe analyses; [f] ΔFeO_{tot}: relative change in FeO_{tot} contents between starting composition and composition of the run product; *: loops pre-saturated with Fe-oxides; [g] $Fe^{3+}/\Sigma Fe$: cationic ratio; [h] $Fe^{3+}/\Sigma Fe$ from conventional Mössbauer spectroscopy; [i] $Fe^{3+}/\Sigma Fe$ from Mössbauer milliprobe; [j] $Fe^{3+}/\Sigma Fe$ calculated with Eq. (1) and the coefficients of Kress and Carmichael (1991); [k] $Fe^{3+}/\Sigma Fe$ calculated with Eq. (6) and the coefficients of Nikolaev et al. (1996) for tholeiitic series; [l] $Fe^{3+}/\Sigma Fe$ calculated with Eq. (6) and the coefficients of Nikolaev et al. (1996) for subalkaline series

analyses, some experiments were performed using four loops with the same starting material, yielding a total charge of about 150 mg.

The oxygen fugacities were set up at four ΔFMQ values: $+1.4$, 0, -1 and -1.9; Table 2). Under such moderate to reducing redox conditions the highly oxidized starting materials must undergo a strong reduction process to attain equilibrium. Therefore we used long run durations, in most cases between 18 and 63 h, which amply exceed the recommended durations of 6 to 9 h (e.g. Thornber et al. 1980; Toplis and Carroll 1995). To test whether equilibrium was achieved, two "reversal" experiments were performed with the composition SC1-P. The oxygen fugacity was first set at $\Delta FMQ = -2$ for 20 h at 1,190°C in order to strongly reduce the sample, and subsequently raised to $\Delta FMQ = 0$ (OS87-R) or $\Delta FMQ = -1$ (OS88-R) at the same temperature to re-equilibrate for 20 h (Table 2).

Subliquidus experiments

The series of experiments under subliquidus temperatures (1,172–1,132°C) was performed with the composition SC1-P. With the purpose of producing coarse-grained samples with melt pockets large enough for Mössbauer milliprobe spectroscopy, the following procedure was employed: the samples were first heated above their liquidus (i.e. T > 1,180°C) for 0.5 h, subsequently cooled to the final temperature at a constant rate of 3°C/h and held at this temperature for 40 to 76 h (Table 2). The initial heating period above the liquidus was omitted only in three experiments with a final temperature above 1,153°C (OS8, OS1b, OS3a; see Table 2). Again, the run durations are much longer than in comparable subliquidus experiments in the literature (e.g. Toplis and Carroll 1995) and are considered to be sufficient to ensure re-equilibration of the ferric-ferrous ratio at the final temperature.

Analytical techniques

Electron microprobe

Glasses and crystalline phases of the quenched run products were analyzed with a CAMECA SX51 electron microprobe operated with an acceleration voltage of 15 kV and a beam current of 20 nA. The counting times were 10 s on the peaks and 5 s on the background.

The standards used were natural albite (Na) and K-feldspar (K) as well as synthetic wollastonite (Ca, Si), corundum (Al), periclase (Mg), hematite (Fe) and rutile (Ti). The raw data were corrected with the "PAP" software package (Pouchou and Pichoir 1985). To avoid Na volatilization under the electron beam, the incident-beam diameter on glass was enlarged to 10 μm. A finely focused beam was used for all other phases.

Wet chemical analysis

The ferrous iron contents of superliquidus samples were analyzed by wet chemistry at the chemical laboratory of the Institut für Geowissenschaften, Universität Potsdam, using a potentiometric method (Wilson 1955). The wet chemical analyses were carried out in duplicate. The U.S.G.S. standard BIR-1 and a geochemical standard from the geological Survey of Japan, JB1-a, were used as references. The values obtained at Potsdam (8.13 wt.% FeO for BIR-1 and 5.71 for JB1-a) compare well with the accepted values (8.34 wt.% for BIR-1, 5.78 for JB1-a). The Fe_2O_3 contents of the glasses were calculated from the difference between total FeO (retrieved with the electron microprobe) and measured FeO contents. The wet chemical FeO values are determined within ± 0.25 wt%. The relative uncertainties for the electron microprobe FeO_{tot} determinations are about 2%. The resulting absolute uncertainties in $Fe^{3+}/\Sigma Fe$ are ± 0.04 to 0.05, which translates into relative uncertainties between 14 and 50% (for oxidized and reduced samples, respectively).

Mössbauer spectroscopy

$Fe^{3+}/\Sigma Fe$ of the glass pockets in products of subliquidus experiments were determined using the Mössbauer milliprobe at Bayerisches Geoinstitut (Bayreuth), which allowed collection of spectra on spots of 100 μm or greater. $Fe^{3+}/\Sigma Fe$ of glassy samples obtained from superliquidus experiments were determined using conventional Mössbauer spectroscopy in either Heidelberg or Bayreuth.

Mössbauer spectroscopy using the milliprobe technique was conducted on samples embedded in epoxy that had already been analyzed using the electron microprobe. The epoxy disks were cut to a thickness of approximately 150 μm, which corresponds to an absorber thickness of approximately 5 mg Fe/cm². A hole drilled in a piece of 25 μm thick Ta foil (which absorbs 99% of 14.4 keV γ-rays) was placed over the region to be studied while looking under an optical microscope. The diameter of the hole varied from 150 to 500 μm, depending on the size of the glass region to be studied. Prior to Mössbauer spectroscopy, the glass region was checked by polarization microscopy to be free of crystals. Glass samples studied using conventional Mössbauer spectroscopy were prepared by grinding to a powder and mounting in 12 mm diameter sample holders, where absorber thicknesses were approximately 5 mg Fe/cm².

Mössbauer spectra were recorded at room temperature (293 K) in transmission mode on a constant acceleration Mössbauer spectrometer with a nominal 1.85 GBq ^{57}Co source in a 6-micron Rh matrix (conventional method) or a nominal 370 MBq ^{57}Co high specific activity source in a 12 μm Rh matrix (milliprobe method). Further details of the milliprobe method are given in McCammon et al. (1991) and McCammon (1994). The velocity scale was calibrated relative to 25 μm α-Fe foil using the positions certified for National

Bureau of Standards standard reference material no. 1541; line widths of 0.28 mm/s (conventional method) and 0.36 mm/s (milliprobe method) for the outer lines of α-Fe were obtained at room temperature. The spectra were fitted using the commercially available fitting programs NORMOS written by R.A. Brand (distributed by Wissenschaftliche Elektronik GmbH, Germany) and RECOIL written by K. Lagarec and D. Rancourt (distributed by Intelligent Scientific Applications Inc, Canada). Collection times for each Mössbauer spectrum were 1–2 days using the conventional source and 1–5 days using the high specific activity source.

The Mössbauer spectra of the glasses examined in this study consist of broad asymmetric doublets, similar to the spectra of most silicate glasses (Fig. 2). Several approaches were used in fitting the spectra to assess the sensitivity of hyperfine parameters to the fitting model, and the final fit comprised an extended Voigt-based analytic lineshape assuming a two-dimensional (2D) Gaussian distribution for both Fe^{2+} and Fe^{3+} (Lagarec and Rancourt 1997). Such a model provides a more realistic approach to the modeling of site-to-site distortions that occur in the iron coordination polyhedra in glasses and has been successfully applied to the analysis of silicate glass spectra (Alberto et al. 1996). We fit Fe^{2+} absorption to a 2D Gaussian distribution with variable parameters, center shift (CS), Gaussian distribution width (σ_{CS}), quadrupole splitting (QS), Gaussian distribution width (σ_{QS}), and correlation between the CS and QS distributions (ρ). The Lorentzian linewidth was constrained in all cases to the natural value (0.097 mm/s) since thin limit spectra were used (see below). For Fe^{3+} absorption, we fit only the variable parameters CS and QS, since Alberto et al. (1996) found both σ_{CS} and ρ to be essentially zero for Fe^{3+} absorption in all samples that they studied. In addition, σ_{QS} was constrained for Fe^{3+} to 0.50 mm/s based on previous data (Alberto et al. 1996), since unrealistic values were obtained otherwise due to the low resolution of Fe^{3+} absorption at low concentrations (Fig. 2). This constraint likely caused a slight overestimation of $Fe^{3+}/\Sigma Fe$ in glasses with low Fe^{3+} concentration, because the degree of variation in next-nearest neighbor environments is more likely to decrease in such glasses (hence lowering σ_{QS}). However since the effect is difficult to estimate, we constrained σ_{QS} to the same value in all glasses, and included the resulting uncertainty in the estimation of errors in the area ratios. To account for thickness effects, we calculated the intrinsic absorber resonance cross section for each sample based on the absorber thickness to generate a thin limit Mössbauer spectrum on which the hyperfine parameter fits were performed (the procedure is part of the RECOIL fitting program).

We did not apply corrections for variable recoil-free fractions of ferrous and ferric iron. Comparison of Mössbauer spectroscopic and wet chemical plus electron microprobe analysis determinations of the oxidation state of iron in silicate glasses show no systematic deviation between the two methods (Mysen et al. 1985b,
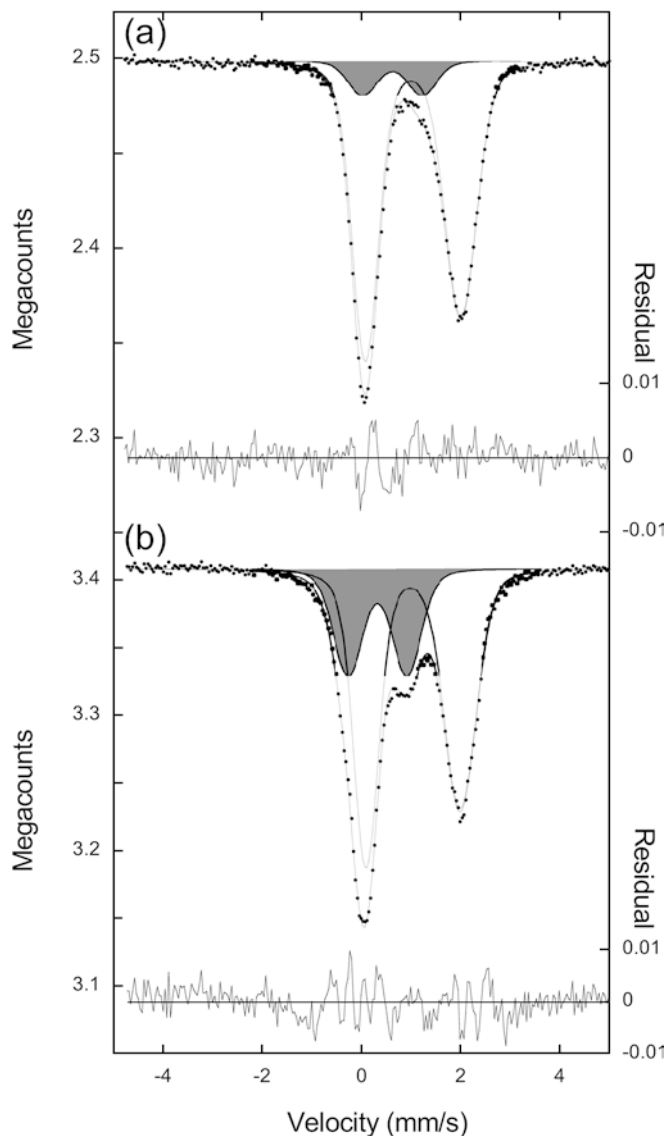

Fig. 2a,b Room temperature ^{57}Fe Mössbauer milliprobe spectra of quenched interstitial glasses in samples synthesized from starting material "SC1-P". *Gray-shaded doublet*: Fe^{3+} absorption, *unshaded doublet*: Fe^{2+} absorption. (**a**) Sample OS21 equilibrated at low fO_2 (ΔFMQ-2), (**b**) Sample OS8 equilibrated at high fO_2 (ΔFMQ+1.3, Table 2)

Dingwell 1991), which suggests that either (1) recoil-free fractions for ferric and ferrous iron in such glasses are similar, or (2) systematic errors in fitting exactly compensate for the effect of differing recoil-free fractions. In support of the first suggestion, low temperature measurements (where recoil-free fraction effects are absent) have shown no difference to room temperature measurements of haplobasaltic glasses, implying similar recoil-free fractions for ferrous and ferric iron (Jayasuriya et al. 2004). However such observations are at odds with suggestions by Ottonello (2001) that Mössbauer spectroscopy overestimates the Fe^{3+} component in glasses due to recoil-free fraction effects. While a definitive answer to this question is still lacking, in this work we

assumed the recoil-free fractions of ferric and ferrous iron to be equal and included effects of this assumption in the estimation of $Fe^{3+}/\Sigma Fe$ uncertainties.

The hyperfine parameters derived from fits according to the above model are listed in the tables, where relative errors were determined using a Monte Carlo approach based on the counting statistics. The relative Fe^{3+} concentrations (listed in Table 2) were determined from the area ratios, and relative errors were estimated based on counting statistics, uncertainties in the fitting model (estimated by fitting the spectra using different models) and the neglect of recoil-free fraction corrections.

Results

Compositional changes and attainment of equilibrium

Two effects may cause changes in the bulk composition of samples equilibrated at high temperatures in gas-mixing furnaces: (1) the loss of alkali metals to the gas stream, and (2) the exchange of iron between sample and platinum wire. Indeed, a few changes are apparent from the compositions of fully glassy products of superliquidus experiments (Tables 2, and 3).

In most run products with bulk composition SC1-P the sodium loss is negligible. The Na_2O contents are only slightly lower than those of the starting material, in fact within the analytical uncertainties ($< 3\%$ relative loss; Table 2). Only in products from runs of longer duration ($t \geq 40$ h) the Na_2O loss was higher (Table 2). In run products of the starting composition 7159V-P the sodium loss increases with decreasing oxygen fugacity and is highest for the product of a run at $\Delta FMQ = -2$ (OS81a, Table 2), which may be related to changes of the melt structure caused by redox changes of iron (see discussion section below).

The exchange of iron between sample and platinum wire depends on the substance used during the pre-saturation procedure of the wire loop. If the starting material was used, subsequent iron loss from the charge

Table 3 Results of electron microprobe analyses (wt.%) of the run products (means and 1σ standard deviation over n single analyses)

ΔFMQ	Run no.	T (°C)	n	SiO₂	TiO₂	Al₂O₃	FeO_tot[a]	MgO	CaO	Na₂O	K₂0	Total
SC1-P												
Superliquidus (T > 1,180 °C)												
+1.4	OS77d	1,221	13	47.60 (13)	2.87 (8)	14.11 (16)	12.90 (27)	6.31 (7)	10.83 (12)	2.75 (7)	0.35 (2)	97.72
	OS89	1,189	20	48.03 (19)	2.85 (9)	14.10 (10)	12.95 (25)	6.28 (7)	10.90 (10)	2.80 (7)	0.37 (3)	98.28
	OS82	1,187	15	47.83 (18)	2.86 (6)	13.77 (12)	12.77 (17)	6.36 (6)	10.85 (17)	2.76 (5)	0.36 (2)	97.56
0	OS79d	1,222	16	47.82 (27)	2.90 (8)	13.85 (14)	12.88 (25)	6.40 (6)	10.88 (14)	2.75 (6)	0.37 (3)	97.84
	OS87R[b]	1,189	14	47.99 (23)	2.89 (8)	14.23 (16)	13.22 (17)	6.33 (8)	10.88 (7)	2.64 (4)	0.34 (4)	98.49
	OS80	1,186	15	47.94 (14)	2.90 (8)	14.05 (16)	12.87 (15)	6.36 (8)	10.83 (12)	2.73 (7)	0.37 (2)	98.03
	OS91	1,185	20	47.63 (47)	2.88 (9)	14.09 (22)	13.26 (28)	6.34 (11)	10.94 (17)	2.77 (7)	0.35 (3)	98.26
−1	OS85	1,188	15	48.34 (20)	2.95 (7)	14.06 (12)	12.37 (22)	6.40 (9)	10.97 (11)	2.63 (8)	0.36 (2)	98.06
	OS88-R	1,188	15	47.83 (25)	2.87 (4)	14.17 (20)	13.30 (19)	6.32 (6)	10.80 (14)	2.82 (8)	0.36 (2)	98.47
	OS90	1,185	20	47.84 (24)	2.87 (9)	14.10 (11)	13.32 (19)	6.36 (9)	10.93 (10)	2.82 (4)	0.35 (2)	98.59
−2	OS81d	1,221	16	47.96 (24)	2.91 (10)	13.86 (17)	12.99 (30)	6.40 (7)	10.88 (11)	2.73 (9)	0.37 (2)	98.10
	OS93-R	1,189	14	47.74 (21)	2.90 (9)	14.20 (19)	13.46 (17)	6.34 (6)	10.78 (13)	2.79 (6)	0.36 (3)	98.57
	OS86	1,188	14	47.92 (23)	2.84 (6)	14.11 (15)	13.19 (18)	6.29 (8)	10.79 (8)	2.83 (6)	0.37 (3)	98.34
	OS84	1,185	15	48.57 (15)	2.92 (6)	14.20 (16)	11.97 (24)	6.38 (7)	10.97 (14)	2.61 (7)	0.35 (2)	97.97
	OS19	1,184	15	48.23 (22)	2.88 (7)	14.18 (9)	12.68 (14)	6.61 (6)	10.55 (8)	2.71 (5)	0.33 (2)	98.18
Subliquidus (T < 1,180 °C)												
+1.4	OS8	1,172	8	48.55 (32)	2.94 (7)	13.46 (28)	13.61 (14)	6.63 (12)	10.78 (6)	2.74 (5)	0.37 (2)	99.08
	OS10	1,162	8	48.55 (33)	2.97 (10)	13.04 (11)	13.74 (19)	6.79 (6)	10.37 (17)	2.76 (5)	0.39 (2)	98.61
0	OS1b	1,174	15	48.18 (44)	2.88 (8)	14.23 (11)	12.44 (39)	6.50 (9)	10.83 (13)	2.70 (9)	0.37 (2)	98.13
	OS3a	1,154	8	48.39 (26)	3.19 (6)	13.06 (10)	13.67 (22)	6.09 (7)	10.24 (11)	2.77 (7)	0.41 (2)	97.82
	OS18	1,132	8	48.84 (16)	3.78 (9)	11.65 (8)	14.82 (27)	5.35 (6)	10.17 (14)	2.77 (3)	0.45 (2)	97.83
−1	OS13	1,149	10	48.93 (30)	3.31 (8)	13.07 (14)	13.48 (20)	6.32 (12)	9.90 (4)	2.69 (9)	0.40 (2)	98.09
−2	OS17	1,151	10	49.16 (30)	3.43 (8)	12.58 (6)	13.94 (26)	6.15 (6)	10.53 (16)	2.17 (4)	0.37 (2)	98.33
	OS21	1,132	10	48.97 (17)	3.83 (9)	11.69 (9)	14.94 (24)	5.41 (7)	10.80 (9)	2.52 (7)	0.43 (2)	98.59
7159V-P												
Superliquidus (T > 1,180 °C)												
+1.4	OS77a	1,221	15	47.96 (16)	3.99 (7)	13.40 (16)	13.88 (20)	3.21 (6)	9.04 (11)	4.65 (11)	1.16 (4)	97.29
	OS68a	1,183	28	48.01 (24)	4.03 (8)	13.15 (18)	14.28 (22)	3.35 (7)	9.10 (12)	4.70 (9)	1.02 (3)	97.64
0	OS79a	1,222	15	48.31 (21)	4.04 (7)	13.36 (13)	14.02 (15)	3.27 (7)	9.38 (10)	4.66 (10)	1.14 (3)	98.18
−1	OS78a	1,221	15	48.28 (19)	4.06 (6)	13.23 (27)	14.18 (18)	3.30 (6)	9.33 (10)	4.55 (10)	1.15 (3)	98.08
	OS70a	1,183	27	48.31 (27)	3.93 (8)	13.25 (19)	14.15 (25)	3.22 (6)	8.99 (10)	4.56 (11)	1.05 (3)	97.46
−2	OS81a	1,221	15	48.48 (23)	4.02 (7)	13.38 (16)	14.13 (17)	3.34 (4)	9.35 (10)	4.36 (17)	1.15 (4)	98.22

[a]Total FeO from electron microprobe analyses;
[b]reversal experiments marked by R; numbers in parentheses indicate 1σ standard deviation on the last digit

to the platinum wire could occur during the high-temperature run. After run durations of less than one day, the charges generally lost less than 1% relative of their original FeO_{tot} content (Table 2). Consistent with previous studies (e.g. Johannes and Bode 1978), iron loss is higher at longer run durations and lower oxygen fugacities (Table 2). In case Fe_2O_3 was employed to presaturate the loops with iron, the run products have higher FeO_{tot} contents than the starting material. The iron gain of the run products seems to be higher in runs of long duration, but did not exceed 4% relative (sample OS93, held 63 h at superliquidus temperature; Table 2). This is in accord with observations of Grove (1981), who showed that the Pt-loop might return iron to the sample when the original iron content of the loop is higher than the equilibrium value of the sample under the desired T-fO_2 conditions.

Our data show no correlation between bulk compositional changes and $Fe^{3+}/\Sigma Fe$ in the glasses (Table 2), which implies that the oxidation state of the samples was influenced primarily by oxygen fugacity as fixed by the CO/CO_2 gas mixtures, provided that equilibrium was attained during the final phase (at constant temperature) of the experiments. We have good indications for a close approach to equilibrium in our experimental charges. First, experiments performed at the same T-fO_2 conditions but with different, long run durations display very similar or identical bulk $Fe^{3+}/\Sigma Fe$ (e.g. products of runs OS86, OS84, OS93 equilibrated at $\Delta FMQ-2$ for 20.5, 45, and 63 h, i.e. with run durations much longer than usually recommended; Table 2). Still more convincing is the good agreement between the results of synthesis and reversal experiments. The bulk $Fe^{3+}/\Sigma Fe$ values are the same within the analytical uncertainties (in Table 2 compare samples OS87-R and OS80, OS88-R and OS85). The durations of our subliquidus runs were as long as or even longer than those considered sufficient to reach equilibrium by Toplis and Carroll (1995) for the same starting composition and T-fO_2 conditions.

Run products

The products of all superliquidus experiments consist of dark brownish glasses (quenched melts), chemically homogeneous within the counting statistics of the electron microprobe (Table 3). The products of the subliquidus experiments contain crystals more or less homogeneously distributed throughout the glassy matrix. Plagioclase crystals are euhedral, have elongated shape and may reach 0.5 mm in length. Olivine crystals have slightly rounded, more bulky shapes. In run products equilibrated at temperatures above 1,130°C, the glassy areas between the crystals (glass pockets) are large enough for measurements with the Mössbauer milliprobe. With decreasing temperature and increasing crystallinity, however, the size of the glass pockets in the

quenched samples decreases, precluding the use of the Mössbauer milliprobe.

Plagioclase, which is the first phase to crystallize on the liquidus between 1,184 and 1,179°C, is present in all quenched charges and has anorthite contents falling with temperature from 72 to 60 mol%. As a result of the cooling procedure between the superliquidus and the final temperature (see section "subliquidus experiments"), the plagioclase crystals are zoned with a maximal compositional range of 8 mol% anorthite within a single charge for a sample equilibrated at 1,132°C (OS18). In contrast, the olivine crystals are practically unzoned (max. compositional range: ± 0.7 mol% forsterite) and the glass domains show constant compositions within each charge (Table 3). Olivine appears on the liquidus below 1,160°C with a composition around Fo_{74} and becomes slightly more fayalitic with decreasing temperature (Fo_{69-70} at 1,132°C).

Melt compositions, liquidus temperatures and olivine compositions are in excellent agreement with the data of Toplis and Carroll (1995) on a similar bulk composition (Fig. 3). In contrast, our observations point to a liquidus temperature for plagioclase at 1,180°C, i.e. 20°C higher than registered by Toplis and Carroll (1995) and to anorthite contents lower by about 5 mol% over the 1,180–1,130°C temperature range. These differences are related to small differences in the bulk composition of the starting material (SC1-P) compared to "SC1" of Toplis and Carroll (1995).

The compositions of the quenched residual melts reflect the crystallization sequence and the increasing degree of crystallization with decreasing final temperature; i.e. the glasses have increasing SiO_2, FeO_{tot} and K_2O but decreasing Al_2O_3, MgO and CaO contents with decreasing temperature (Table 3). All quenched residual liquids have, nevertheless, basaltic compositions.
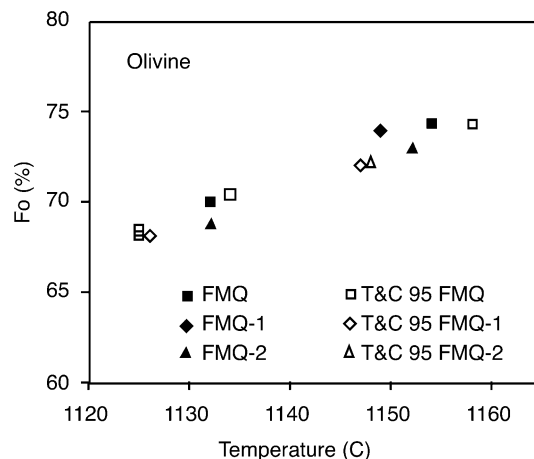

Fig. 3 Forsterite contents (in mol%) of olivine as a function of temperature in run products from the present work (*filled symbols*) compared to those from Toplis and Carroll (1995) (*open symbols*)

Chemical vs. Mössbauer determination of $Fe^{3+}/\Sigma Fe$ in glass

Equations (1) and (6) were calibrated on the basis of $Fe^{3+}/\Sigma Fe$ values retrieved from combined wet chemical and electron microprobe analyses. Because the $Fe^{3+}/\Sigma Fe$ values used in the present study are derived from broadened Mössbauer spectra, it is important to show that these values are consistent with those obtained by wet chemical analysis. Such comparisons have already been performed on a wide compositional variety of quenched silicate glasses and showed no systematic bias in the results from either of the two techniques (Mysen et al. 1985b, Dingwell 1991), but we nevertheless chose to test our results with a few chemical analyses.

Four samples equilibrated at superliquidus temperatures and four different fO_2s (OS89, OS91, OS90, OS86; Table 2) were analyzed both with the electron microprobe (for total Fe) and with wet chemistry (for Fe^{2+}). Each of them is fully comparable with samples synthesized under identical T-fO_2 conditions that were examined with Mössbauer spectroscopy. For the samples equilibrated at oxygen fugacities between $\Delta FMQ = -2$ and $\Delta FMQ = 0$ the agreement between the $Fe^{3+}/\Sigma Fe$ values derived using Mössbauer spectroscopy and wet chemical analysis is excellent (Table 2, Fig. 4). For the samples equilibrated at $\Delta FMQ + 1.4$, the values just overlap within the uncertainties (Table 2, Fig. 4); however we suspect that sample OS89 might have experienced higher fO_2 due to a technical problem during the run. In summary, we consider the $Fe^{3+}/\Sigma Fe$ values determined using Mössbauer spectroscopy to constitute a realistic basis for comparison with the numbers calculated from the empirical equations.
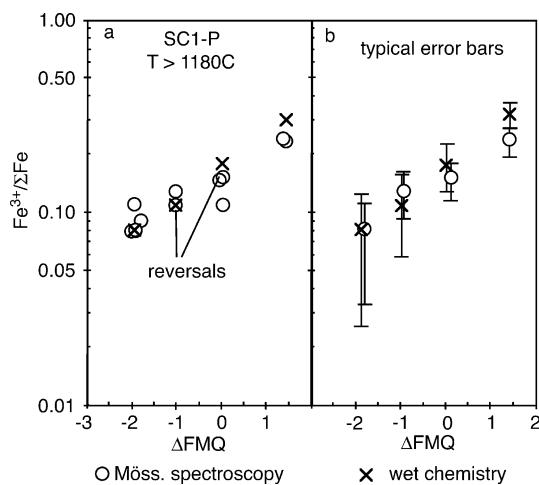
Calculated versus measured $Fe^{3+}/\Sigma Fe$ in glasses

In the following we consider measured $Fe^{3+}/\Sigma Fe$ values to those determined using Mössbauer spectroscopy, performed either with a conventional spectrometer or with the milliprobe technique. The calculated $Fe^{3+}/\Sigma Fe$ values were obtained by plugging the experimental temperature, oxygen fugacity and chemical composition of the quenched glasses into one of the empirical equations. We used Eq. (1) with the coefficients derived by Kress and Carmichael (1991) and Eq. (6) with the coefficients proposed by Nikolaev et al. (1996) for the tholeiitic series (bulk composition SC1-P) and the subalkaline series (7159V-P) (Table 4). For both equations, the $Fe^{3+}/\Sigma Fe$ uncertainties result from the experimental (temperature: $\pm 2°C$, log fO_2: ± 0.2) and analytical (1% relative for each oxide component) uncertainties, and can be estimated to be roughly ± 0.01 at low fO_2 ($\Delta FMQ = -2$) and up to ± 0.02 at high fO_2 ($\Delta FMQ = +1.4$).

We did not take into account the quality of the calibrations as given in the original papers of Kress and Carmichael (1991) and Nikolaev et al. (1996). The ferric-ferrous ratios (Fe^{3+}/Fe^{2+}) back calculated with Eq. (6) are reproducible to a precision of 0.03 (tholeiitic series) or 0.04 (subalkaline series) (Nikolaev et al. 1996), corresponding to a precision in $Fe^{3+}/\Sigma Fe$ of 0.02–0.03. Kress and Carmichael (1991) give only standard errors for the calculation of FeO (0.21 wt%) and Fe_2O_3 (0.42 wt%). Using these values, the absolute uncertainties of $Fe^{3+}/\Sigma Fe$ are calculated to be 0.01–0.1, depending on the ferric and ferrous iron concentrations in the quenched melt.

Ferrobasaltic bulk composition "SC1-P"

The $Fe^{3+}/\Sigma Fe$ values measured on the synthetic glasses display a clear positive correlation with experimental oxygen fugacity (ΔFMQ), both under superliquidus (Fig. 5a) and subliquidus conditions (Fig. 5c). Within the uncertainties (Fig. 5b), the experimental $Fe^{3+}/\Sigma Fe$ values match well with those calculated with the model of Kress and Carmichael (1991) over the entire fO_2 range, showing deviations of generally 0.03 or less (Figs. 5a,c, and 6a).

Fig. 4a,b (a) $Fe^{3+}/\Sigma Fe$ in glasses synthesized at superliquidus conditions from starting material "SC1-P" as a function of oxygen fugacity (ΔFMQ). Comparison of the values determined from a combination of wet chemical and electron microprobe analyses or using Mössbauer spectroscopy. **(b)** Typical uncertainty bars for $Fe^{3+}/\Sigma Fe$

Table 4 Regression coefficients for Eqs. 1 and 6

	Eq. (1) Kress and Carmichael (1991)	Eq. (6) Nikolaev et al. (1996)	
		Tholeiitic (I)	Subalkaline (II)
a	0.196	0.1395	0.1817
b	11492	3282.2	4348.4
c	−6.675		
d_{SiO2}		−1.4238	−2.5966
d_{TiO2}		−4.3585	3.7652
d_{Al2O3}	−2.243	−9.4488	−1.3025
d_{FeOtot}	−1.828	−0.755	−3.9708
d_{MgO}		−2.2326	−3.9808
d_{CaO}	3.201	0.3404	−0.4226
d_{Na2O}	5.854	2.4766	0.5992
d_{K2O}	6.215	4.4534	0.1417

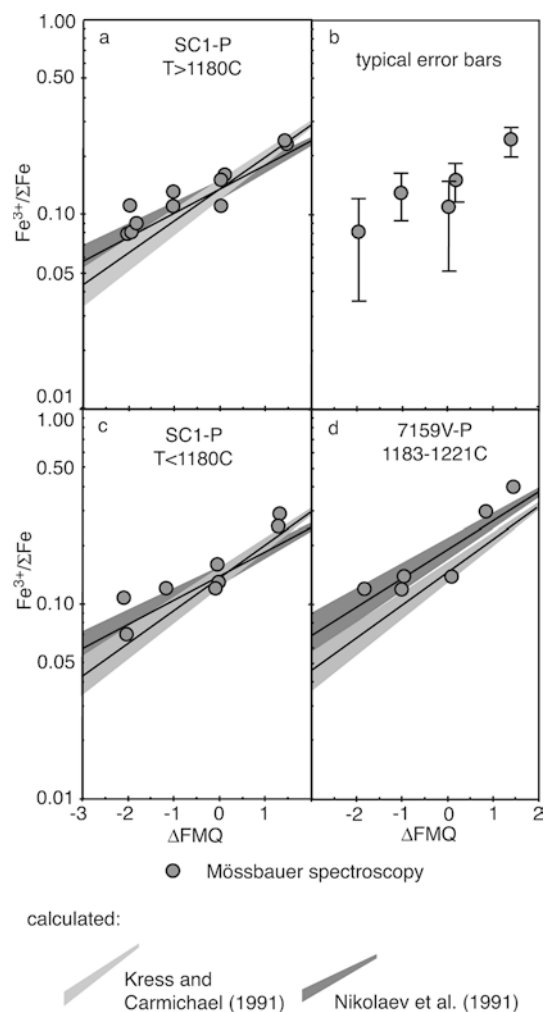**Fig. 5a–d** Variation of $Fe^{3+}/\Sigma Fe$ with oxygen fugacity in synthetic glasses, comparing values measured using Mössbauer spectroscopy with those calculated using the equations of Kress and Carmichael (1991) and Nikolaev et al. (1996) (*lines + shaded areas* for the uncertainties). (**a**) Results of superliquidus experiments on composition SC1-P. (**b**) Typical error bars for the Mössbauer spectroscopic $Fe^{3+}/\Sigma Fe$ determinations. (**c**) Results of subliquidus experiments on bulk composition SC1-P. (**d**) Results of superliquidus experiments on composition 7159V-P

Fig. 6a,b Differences between measured (Mössbauer) and calculated $Fe^{3+}/\Sigma Fe$ for glasses equilibrated at super- or subliquidus conditions on bulk composition "SC1-P" as a function of equilibration temperature and oxygen fugacity. (**a**) Calculations using Eq. (1) and the coefficients of Kress and Carmichael (1991). (**b**) Calculations using Eq. (6) and the coefficients proposed for the tholeiitic series (Nikolaev et al. 1996)

In the low oxygen fugacity range (ΔFMQ −2 to 0), the equation of Nikolaev et al. (1996) reproduces the measured $Fe^{3+}/\Sigma Fe$ values as well as, or even better, than the model of Kress and Carmichael (1991), with deviations generally less than 0.02 (Figs. 5a, c, and 6b). However this equation is less successful in modeling the experimental data at the highest fO_2. In the latter case, the calculated values are higher than the measured ones, particularly at subliquidus conditions where deviations exceed 0.04, although most values still overlap within uncertainties (Figs. 5a, c, and 6b).

Transitional alkali basaltic bulk composition 7159V-P

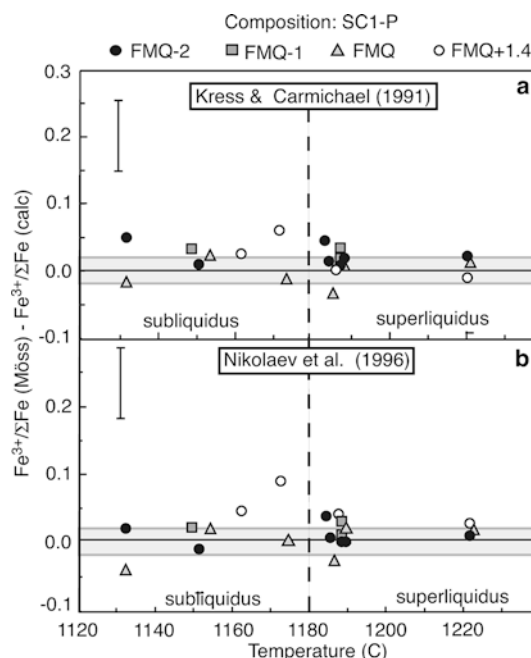In case of the more alkalic bulk composition, the model of Kress and Carmichael (1991) [Eq. (1)] slightly underestimates glass $Fe^{3+}/\Sigma Fe$ at low fO_2, where the greatest deviation (0.05) occurs at the lowest fO_2. Agreement improves with increasing fO_2 up to roughly ΔFMQ, but the calculated values again underestimate $Fe^{3+}/\Sigma Fe$ at $\Delta FMQ \geq 1$, reaching a maximum deviation of 0.15 at the highest fO_2 (Fig. 5d). In contrast, the model of Nikolaev et al. (1996) reproduces the experimental data reasonably well up to $\Delta FMQ 3+/\Sigma Fe$ at the highest fO_2 (Fig. 5d).

Discussion

Comparison between the calculation models

The good agreement between the experimental $Fe^{3+}/\Sigma Fe$ values of the glasses on bulk composition SC1-P and the results of the calculations using both equations (Kress and Carmichael 1991, Nikolaev et al. 1996) is very encouraging and suggests that the corresponding equations can be used at temperatures distinctly lower than those of their calibrations (Fig. 6). Furthermore, the correlation lines between log $Fe^{3+}/\Sigma Fe$ and ΔFMQ calculated with both models fit the experimental data, implying that the fO_2 dependency of the ferric-ferrous ratio is satisfactorily calibrated.

Ariskin and Barmina (1999) pointed out that experimental data under highly oxidized conditions are over-represented in the database used to calibrate

Eq. (1) (Fig. 1), resulting in a systematic underestimation of the $Fe^{3+}/\Sigma Fe$ of glasses at low oxygen fugacities (cf. also Nikolaev et al. 1996). Our results, however, show the contrary. The agreement between the experimental $Fe^{3+}/\Sigma Fe$ values and those calculated with the equation of Kress and Carmichael (1991) is quite good at low to moderate fO_2 (Figs. 5a, b, and 6a).

Nikolaev et al. (1996) calibrated their equation on only part of the experimental data used by Kress and Carmichael (1991), omitting all runs equilibrated at $\Delta FMQ > +1.7$ to avoid the influence of results obtained under highly oxidized conditions. Apparently this approach is not successful, since calculated and measured $Fe^{3+}/\Sigma Fe$ show greater deviation at high fO_2 (Fig. 6b).

Nikolaev et al. (1996) also stated that the accuracy of ferric-ferrous ratios calculated with Eq. (1) is dependent on melt compositions. Indeed, the model of Kress and Carmichael (1991) better reproduces the measured $Fe^{3+}/\Sigma Fe$ of glasses from the ferrobasaltic bulk composition SC1-P than those for the transitional alkalic composition 7159V-P (Figs. 5d, and 7a). Using the calibration coefficients proposed by Nikolaev et al. (1996) for subalkaline compositions improves the calculated results for 7159V-P, but only for low to moderate ferric-ferrous ratios (Fig. 7c). None of the models can reproduce the $Fe^{3+}/\Sigma Fe$ values for moderately alkali-basaltic liquids equilibrated at high fO_2.

Alkalic vs. tholeiitic bulk compositions

The ferric-ferrous ratio of silicate melts is known to increase with increasing sodium and potassium content (e.g. Thornber et al. 1980; Dickenson and Hess 1986). Therefore, it is not surprising that the glasses synthesized from the transitional alkalic composition (7159V-P) with nearly twice as much alkalis as the ferrobasaltic composition (SC1-P; Table 1), also have much higher $Fe^{3+}/\Sigma Fe$ at the same T and fO_2 (Table 2, Fig. 5). The differences between the ferric-ferrous ratios of the glasses for the two bulk compositions increase with increasing fO_2, such that the greatest difference in $Fe^{3+}/\Sigma Fe$ occurs at the most oxidizing conditions ($\Delta FMQ = +1.4$). These observations can be explained by considerations of the melt structure.

As shown in Table 5, the hyperfine parameters for Fe^{2+} in all our glasses indicate octahedral coordination (e.g. Dyar 1985), independent of glass composition and of the oxygen fugacity during the high temperature equilibration. For the most oxidized samples, center shift and quadrupole splitting values suggest ferric iron in an environment with coordination lower than six (Table 5) (e.g. Dyar 1985). The isomer shift for ferric iron increases with decreasing $Fe^{3+}/\Sigma Fe$ (Fig. 8), which is consistent with previous observations. The decrease has been explained by a change from tetrahedrally to octahedrally coordinated ferric iron (Mysen et al. 1980; Virgo and Mysen 1985; Mysen et al. 1985a).
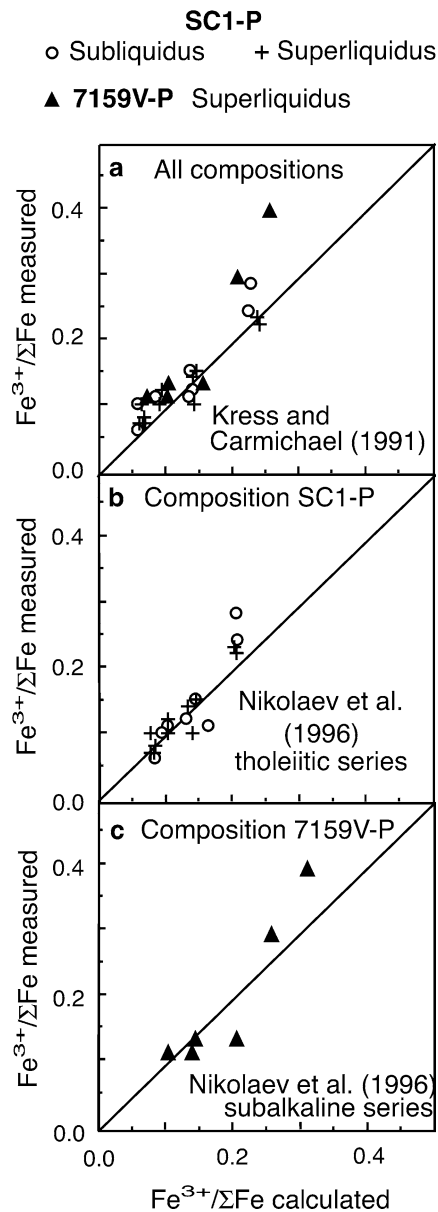

Fig. 7a–c Measured (Mössbauer) versus calculated $Fe^{3+}/\Sigma Fe$ in glasses equilibrated at super- or subliquidus conditions from bulk compositions SC1-P (a and b) and 7159V-P (a and c). (a) Calculations using Eq. (1) and the coefficients of Kress and Carmichael (1991); (b) Calculations using Eq. (6) and the coefficients proposed for the tholeiitic series; (c) Calculations using Eq. (6) and the coefficients proposed for the subalkaline series

The local charge balance of tetrahedrally coordinated Fe^{3+} must be maintained by network modifying cations (Na^+, K^+, Ca^{2+}). Hence, glasses with higher alkali contents (e.g. composition 7159V-P) can be expected to accommodate more ferric iron in tetrahedral coordination at high oxygen fugacities than glasses with low alkali contents (e.g. composition SC1-P). In contrast, at low fO_2 octahedrally coordinated Fe^{3+} should be less dependent on the alkali content of the melt, resulting in only small differences between the ferric-ferrous ratios of both starting compositions (Table 2, Fig. 4). However,

Table 5 Hyperfine parameters derived from fits to room temperature Mössbauer spectra

ΔFMQ	Run no.	T (°C)		CS (mm/s)	σ (mm/s)	QS (mm/s)	σ (mm/s)	ρ (mm/s)	Area
SC1-P Superliquidus (T > 1,180 °C)									
+1.4	OS77d	1,221	Fe^{2+}(VI)	1.036 (1)	0.22 (1)	1.943 (23)	0.24 (1)	0.35 (9)	0.77 (5)
			Fe^{3+}	0.29 (6)		1.09 (9)	*0.50*		0.23 (5)
	OS82	1,187	Fe^{2+}(VI)	1.030 (6)	0.22 (1)	1.888 (9)	0.28 (2)	0.37 (4)	0.76 (4)
			Fe^{3+}	0.33 (2)		1.18 (4)	*0.50*		0.24 (4)
0	OS79d	1,222	Fe^{2+}(VI)	1.020 (16)	0.21 (1)	1.942 (30)	0.25 (2)	0.29 (5)	0.84 (4)
			Fe^{3+}	0.51 (9)		0.91 (17)	*0.50*		0.16 (4)
	OS87−R	1,189	Fe^{2+}(VI)	1.038 (10)	0.27 (1)	1.944 (20)	0.07 (2)	0.49 (10)	0.85 (4)
			Fe^{3+}	0.55 (7)		1.07 (10)	*0.50*		0.15 (4)
	OS80	1,186	Fe^{2+}(VI)	1.026 (9)	0.21 (1)	1.897 (14)	0.26 (1)	0.29 (6)	0.89 (4)
			Fe^{3+}	0.29 (8)		0.88 (16)	*0.50*		0.11 (4)
−1	OS85	1,188	Fe^{2+}(VI)	1.042 (17)	0.23 (1)	1.911 (26)	0.30 (2)	0.17 (9)	0.87 (4)
			Fe^{3+}	0.59 (10)		1.16 (22)	*0.50*		0.13 (4)
	OS88-R	1,188	Fe^{2+}(VI)	1.048 (31)	0.26 (1)	1.903 (11)	0.08 (1)	0.67 (5)	0.89 (4)
			Fe^{3+}	0.56 (5)		*1.2*	*0.50*		0.11 (4)
−2	OS81d	1,221	Fe^{2+}(VI)	1.045 (19)	0.22 (1)	1.917 (25)	0.23 (4)	0.38 (7)	0.91 (4)
			Fe^{3+}	0.61 (23)		1.26 (41)	*0.50*		0.09 (4)
	OS93-R	1,189	Fe^{2+}(VI)	1.047 (3)	0.26 (1)	1.911 (8)	0.09 (1)	0.73 (3)	0.92 (4)
			Fe^{3+}	0.59 (5)		*1.2*	*0.50*		0.08 (4)
	OS86	1,188	Fe^{2+}(VI)	1.050 (2)	0.27 (1)	1.912 (6)	0.09 (1)	0.74 (3)	0.92 (4)
			Fe^{3+}	0.58 (5)		*1.2*	*0.50*		0.08 (4)
	OS84	1,185	Fe^{2+}(VI)	1.043 (11)	0.24 (1)	1.902 (26)	0.32 (1)	0.22 (7)	0.92 (4)
			Fe^{3+}	0.58 (17)		1.09 (28)	*0.50*		0.08 (4)
	OS19	1,184	Fe^{2+}(VI)	1.045 (5)	0.26 (1)	1.916 (12)	0.09 (1)	0.64 (4)	0.89 (5)
			Fe^{3+}	0.48 (7)		1.18 (11)	*0.50*		0.11 (5)
Subliquidus (1,132–1,174 °C)									
+1.4	OS8	1,172	Fe^{2+}(VI)	1.045 (4)	0.25 (1)	1.898 (7)	0.08 (1)	0.94 (4)	0.71 (5)
			Fe^{3+}	0.33 (1)		1.19 (2)	*0.50*		0.29 (5)
	OS10	1,162	Fe^{2+}(VI)	1.049 (6)	0.26 (1)	1.903 (10)	0.10 (1)	0.83 (5)	0.75 (4)
			Fe^{3+}	0.34 (3)		1.19 (5)	*0.50*		0.25 (4)
0	OS1b	1,174	Fe^{2+}(VI)	1.012 (15)	0.18 (1)	1.985 (22)	0.07 (2)	0.63 (16)	0.87 (4)
			Fe^{3+}	0.42 (9)		0.92 (19)	*0.50*		0.13 (4)
	OS3a	1,154	Fe^{2+}(VI)	1.047 (7)	0.24 (1)	1.865 (12)	0.08 (1)	0.84 (7)	0.84 (4)
			Fe^{3+}	0.36 (5)		1.29 (8)	*0.50*		0.16 (4)
	OS18	1,132	Fe^{2+}(VI)	1.046 (9)	0.25 (1)	1.914 (16)	0.08 (1)	0.98 (5)	0.88 (3)
			Fe^{3+}	0.41 (8)		1.14 (15)	*0.50*		0.12 (3)
−1	OS13	1,149	Fe^{2+}(VI)	1.056 (13)	0.25 (1)	1.910 (27)	0.17 (2)	0.33 (7)	0.88 (4)
			Fe^{3+}	0.58 (13)		1.24 (24)	*0.50*		0.12 (4)
−2	OS17	1,151	Fe^{2+}(VI)	1.045 (7)	0.25 (1)	1.901 (19)	0.16 (3)	0.56 (5)	0.93 (4)
			Fe^{3+}	0.59 (16)		*1.2*	*0.50*		0.07 (4)
	OS21	1,132	Fe^{2+}(VI)	1.044 (2)	0.25 (1)	1.927 (7)	0.08 (1)	0.68 (3)	0.89 (5)
			Fe^{3+}	0.63 (3)		*1.2*	*0.50*		0.11 (5)
7159V Superliquidus (1,183–1,222 °C)									
+1.4	OS77a	1,221	Fe^{2+}(VI)	1.012 (10)	0.25 (1)	1.919 (17)	0.08 (1)	0.94 (11)	0.60 (6)
			Fe^{3+}	0.31 (1)		1.14 (4)	*0.50*		0.40 (6)
	OS68a	1,183	Fe^{2+}(VI)	1.041 (8)	0.27 (1)	1.876 (13)	0.10 (1)	0.81 (7)	0.70 (5)
			Fe^{3+}	0.33 (2)		1.21 (3)	*0.50*		0.30 (5)
0	OS79a	1,222	Fe^{2+}(VI)	1.013 (10)	0.29 (1)	1.903 (18)	0.08 (1)	0.67 (8)	0.86 (4)
			Fe^{3+}	0.51 (5)		1.02 (9)	*0.50*		0.14 (4)
−1	OS78a	1,221	Fe^{2+}(VI)	1.033 (14)	0.27 (1)	1.881 (27)	0.08 (1)	0.84 (14)	0.86 (4)
			Fe^{3+}	0.42 (13)		1.19 (23)	*0.50*		0.14 (4)
	OS70a	1,183	Fe^{2+}(VI)	1.025 (7)	0.29 (1)	1.895 (14)	0.07 (1)	0.69 (8)	0.88 (4)
			Fe^{3+}	0.53 (5)		1.03 (10)	*0.50*		0.12 (4)
−2	OS81a	1,221	Fe^{2+}(VI)	1.014 (7)	0.29 (1)	1.895 (19)	0.08 (1)	0.71 (8)	0.88 (4)
			Fe^{3+}	0.52 (6)		0.97 (14)	*0.50*		0.12 (4)

CS: centre shift (relative to α-Fe); QS: quadrupole splitting; σ: Gaussian line width; ρ: correlation; numbers in parentheses indicate the 1σ standard deviation of the final digit; numbers in italics indicate parameters that were held fixed during fitting
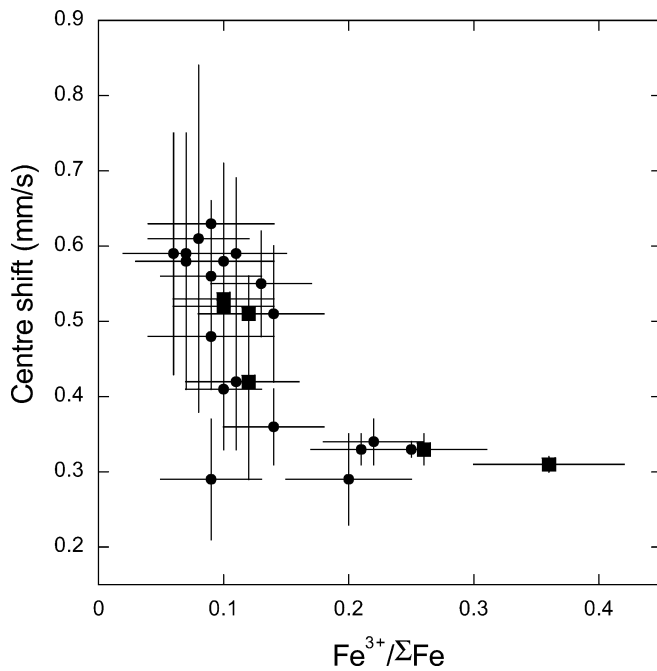
Fig. 8 Variation of Fe^{3+} center shift (relative to α-Fe) with $Fe^{3+}/\Sigma Fe$ for all glasses (*circles*: SC1-P; *squares*: 7159V-P)

assignments of Fe^{2+} and Fe^{3+} to discrete coordination polyhedra probably represent an oversimplification for glasses. The Fe site environment in glasses is not distinct as for crystals, but rather varies from site to site, which is reflected in the distribution of hyperfine parameters.

fO_2 estimates from $Fe^{3+}/\Sigma Fe$ of natural glasses

Equations (1) and (6) are frequently used to calculate magmatic oxygen fugacities from volcanic glasses. In order to assess the uncertainties of such fO_2 estimates, we recast our data in terms of $\log fO_2$ and compared the calculated oxygen fugacities with the ones actually maintained during the equilibration of the sample material (Fig. 9). The uncertainties of the calculated $\log fO_2$ values are about ± 0.5 log units as estimated from the experimental uncertainties (temperature: ± 2 °C), electron microprobe analysis uncertainties (1% relative for each oxide component) and Mössbauer-determined $Fe^{3+}/\Sigma Fe$ uncertainties (roughly 0.04). On the whole, both equations reproduce the experimental fO_2 with similar accuracy. The mean deviation between observed and calculated fO_2s for all samples is only 0.5 log-bar unit, and maximum deviations rarely exceed one log-bar unit. Both models tend to underestimate the oxygen fugacity (Fig. 9), but the equation of Nikolaev et al. (1996) systematically yields too low values at $\Delta FMQ \leq 0$.

Hence, Eq. (1) is suitable for the estimation of magmatic oxygen fugacities and Eq. (6) is suitable for the calculation at low to moderate oxygen fugacities with an accuracy of generally better than one log-bar unit. But
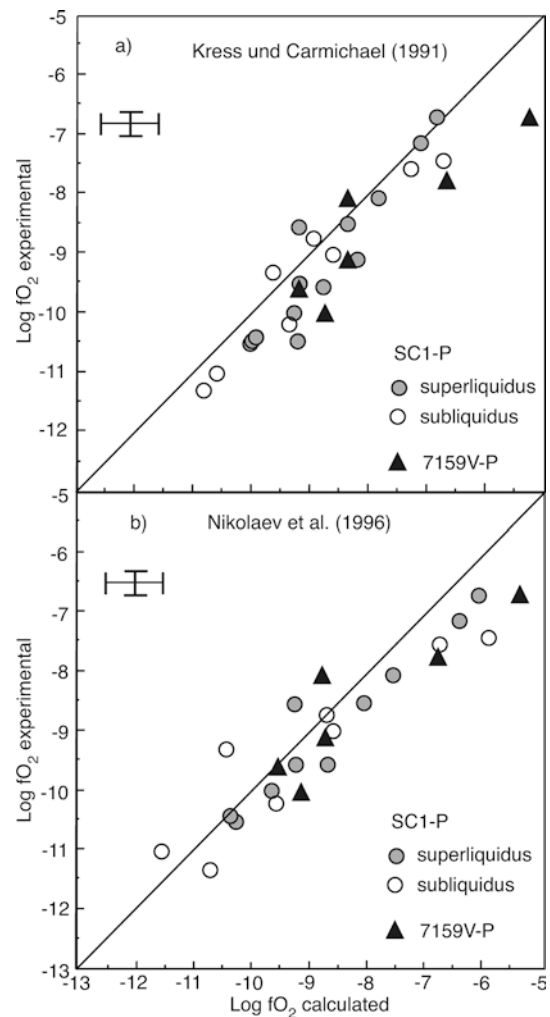

Fig. 9a,b Experimental versus calculated fO_2 in glasses equilibrated at super- or subliquidus conditions from bulk compositions SC1-P and 7159V-P. (**a**) Calculated using Eq. (1) (Kress and Carmichael 1991); (**b**) Calculated using Eq. (6) (Nikolaev et al. 1996)

care has to be taken regarding the composition of natural samples, because the accuracy of the calculation likely varies for different compositions. On the other hand the effect of temperature on the calculated oxygen fugacities is small if oxygen fugacities relative to a buffer are considered (ΔFMQ) and thus an exact knowledge of the temperature in the magma is not required.

Conclusion

In the present study we have tested whether the equations of Kress and Carmichael (1991) and Nikolaev et al. (1996) that relate oxygen fugacity to $Fe^{3+}/\Sigma Fe$ in quenched liquids are accurate at temperatures around and below 1,200 °C, i.e. on the boundary or outside the range of the equation calibrations. We found that the temperature dependence for both equations seems to be adequately accounted for. In particular, both models

successfully reproduce $Fe^{3+}/\Sigma Fe$ of the quenched liquids of the ferrobasaltic bulk composition SC1-P to within 0.05.

The models are less successful in accommodating different bulk compositions. For instance, the equation of Kress and Carmichael (1991) shows larger deviations from measured values for quenched liquids with transitional alkali-basaltic compositions. The model of Nikolaev et al. (1996), which proposed different coefficients for different compositional series, generally yields better results for this composition, except at high fO_2 conditions in which $Fe^{3+}/\Sigma Fe$ is clearly underestimated. In this special case, $Fe^{3+}/\Sigma Fe$ estimates can deviate from the actual values by as much as 0.1, and the corresponding relative fO_2 (ΔFMQ) determinations by more than one order of magnitude. An experimental check using the bulk composition of interest is therefore highly recommended.

References

Alberto HV, Pinoto da Cunha JL, Mysen BO, Gil JM, Ayres de Campos N (1996) Analysis of Mössbauer spectra of silicate glasses using a two-dimensional Gaussian distribution of hyperfine parameters. J Non-Cryst Solids 194:48–57

Ariskin AA, Barmina GS (1999) An empirical model for the calculation of spinel-melt equilibria in mafic igneous systems at atmospheric pressure: 2. Fe.Ti oxides. Contrib Mineral Petrol 134:251–263

Borisov A (1988) Temperature dependence of redox reactions involving variable-valency elements in model and natural melts. Geochem Int 25:85–93

Borisov AA, Shapkin AI (1990) A new empirical equation relating the Fe^{3+}/Fe^{2+} ratio in natural melts to composition, oxygen fugacity and temperature. Geochem Int 27:111–116

Brooks CK, Nielsen TFD (1978) Early stages in the differentiation of the Skaergaard magma as revealed by a closely related suite of dyke rocks. Lithos 11:1–14

Deines P, Nafziger RH, Ulmer GC, Woermann E (1974) Temperature-oxygen fugacity tables for selected gas mixtures in the system C-H-O at one atmosphere total pressure. Bull Earth Mineral Sci Exp Sta, Penn State Univ, 128 pp

Dickenson MP, Hess PC (1986) The structural role and homogeneous redox equilibria of iron in peraluminous, metaluminous and peralkaline silicate melts. Contrib Mineral Petrol 92(2):207–217

Dingwell DB (1991) Redox viscometry of some Fe-bearing silicate melts. Am Mineral 76:1560–1562

Dingwell DB, Brearley M (1988) Melt densities in the CaO-FeO-Fe_2O_3-SiO_2 system and the compositional dependence of the partial molar volume of ferric iron in silicate melts. Geochim Cosmochim Acta 52:2815–2825

Dingwell DB, Virgo D (1987) The effect of oxidation state on the viscosity of melts in the system Na_2O-FeO-Fe_2O_3-SiO_2. Geochim Cosmochim Acta 51:195–205

Dyar MD (1985) A review of Mössbauer data on inorganic glasses: the effects of composition on iron valency and coordination. Am Mineral 70:304–316

Fudali RF (1965) Oxygen fugacities of basaltic and andesitic magmas. Geochim Cosmochim Acta 29:1063–1075

Ford CE (1978) Platinum-iron alloy sample containers for melting experiments on iron-bearing rocks, minerals, and related systems. Mineral Mag 42:271–275

Grove TL (1981) Use of FePt alloys to eliminate the iron loss problem in 1 atmosphere gas mixing experiments: theoretical and practical considerations. Contrib Mineral Petrol 78:298–304

Jayasuriya KD, O'Neill HSC, Berry AJ, Campbell SJ (2004) A Mössbauer study of the oxidation state of iron in silicate melts. Am Mineral (submitted)

Johannes W, Bode B (1978) Loss of iron to the Pt-container in melting experiments with basalts and a method to reduce it. Contrib Mineral Petrol 67:221–225

Kennedy GS (1948) Equilibrium between volatiles and iron oxides in igneous rocks. Am J Sci 246:529–549

Kilinc A, Carmichael ISE, Rivers ML, Sack RO (1983) The ferric-ferrous ratios of natural silicate liquids equilibrated in air. Contrib Mineral Petrol 83:136–140

Kress VC, Carmichael ISE (1988) Stoichiometry of the iron oxidation reaction in silicate melt. Am Mineral 73:1267–1274

Kress VC, Carmichael ISE (1991) The compressibility of silicate liquids containing Fe_2O_3 and the effect of composition, temperature, oxygen fugacity and pressure on their redox states. Contrib Mineral Petrol 108:82–92

Lagarec K, Rancourt DG (1997) Extended Voigt-based analytic lineshape method for determining N-dimensional correlated hyperfine parameter distributions in Mössbauer spectroscopy. Nucl Instr Meth Phys Res B 129:266–280

Lattard D, Partzsch GM (2001) Magmatic crystallization experiments at 1 bar in systems closed to oxygen: A new/old experimental approach. Eur J Mineral 13:467–478

Luhr JF, Carmichael ISE (1985) Jorullo Volcano, Michoacán, Mexico (1759–1774): The earliest stages of fractionation in calc-alkaline magmas. Contrib Mineral Petrol 90:142–161

McCammon CA (1994) A Mössbauer milliprobe: Practical considerations. Hyperfine Int 92:1235–1239

McCammon CA, Chaskar V, Richards GG (1991) A technique for spatially resolved Mössbauer spectroscopy applied to quenched metallurgical slags. Meas Sci Technol 2:657–662

Mysen BO (1987) Magmatic silicate melts: Relations between bulk composition, structure and properties. In: Mysen BO (ed) Magmatic processes: Physicochemical principles. Geochem Soc Spec Publ 1, University Park, pp 375–399

Mysen BO (1991) Relation between structure, redox equilibria of iron, and properties of magmatic liquids. In: Perchuk LL and Kushiro I (eds) Physical chemistry of magmas. Advances in physical geochemistry 9, Springer, New York, pp 41–98

Mysen BO, Virgo D (1983) Effect of pressure on the structure of ion-bearing silicate melts. Carnegie Inst Washington Year Book 82:321–325

Mysen BO, Seifert F, Virgo D (1980) Structure and redox equilibria of iron-bearing silicate melts. Am Mineral 65:867–884

Mysen BO, Seifert F, Virgo D (1984) Redox equilibria of iron in alkaline earth silicate melts: relationships between structure, oxygen fugacity, temperature and properties of iron-bearing silicate liquids. Am Mineral 69:834–847

Mysen BO, Virgo V, Neuman E-R, Seifert FA (1985a) Redox equilibria and the structural states of ferric and ferrous iron in melts in the system CaO-MgO-Al_2O_3-SiO_2-Fe-O: relationships between redox equilibria, melt structure and liquid phase equilibria. Am Mineral 70:317–331

Mysen BO, Carmichael, ISE, Virgo D (1985b) A comparison of iron redox ratios in silicate glasses determined by wet-chemical and ^{57}Fe Mössbauer resonant absorption methods. Contrib Mineral Petrol 90:101–106

580

Nikolaev GS, Borisov AA, Ariskin AA (1996) Calculation of the ferric-ferrous ratio in magmatic melts: Testing and additional calibration of empirical equations for various magmatic series. Geochem Int 34:641–649

O'Neill HSC (1987) Free energies of formation of NiO, CoO, Ni_2SiO_4, and $CoSiO_4$. Am Mineral 72:280–291

O'Neill HSC (1988) Systems Fe-O and Cu-O: Thermodynamic data for the equilibria Fe-"FeO", $Fe-Fe_3O_4$, "FeO"-Fe_3O_4, Fe_3O_4-Fe_2O_3, $Cu-Cu_2O$, and Cu_2O-CuO from emf measurements. Am Mineral 73:470–486

Ottonello G, Moretti R, Marini L, Zuccolini MV (2001) Oxidation state of iron in silicate glasses and melts: a thermochemical model. Chem Geol 174(1–3):157–179

Pouchou JL, Pichoir F (1985) 'PAP' $\phi(\rho Z)$ procedure for improved quantitative microanalysis. Microbeam Anal 1985:104–106

Presnall DC, Brenner NL (1974) A method for studying iron silicate liquids under reducing conditions with negligible iron loss. Geochim Cosmochim Acta 38:1785–1788

Sack RO, Carmichael ISE, Rivers M, Ghiorso MS (1980) Ferric-ferrous equilibria in natural silicate liquids at 1 bar. Contrib Mineral Petrol 75:369–376

Seifert FA, Virgo D, Mysen BO (1979) Melt structures and redox equilibria in the system Na_2O-FeO-Fe_2O_3-Al_2O_3-SiO_2. Carnegie Inst Washington Year Book 78:511–519

Shibata K (1967) The oxygen partial pressure of the magma from Mihara Volcano, Oshima, Japan. Bull Chem Soc Jpn 40:830–834

Snyder D, Carmichael ISE, Wiebe RA (1993) Experimental study of liquid evolution in an Fe-rich, layered mafic intrusion: constraints of Fe-Ti oxide precipitation on the T-fO_2 and T-ρ paths of tholeiitic magmas. Contrib Mineral Petrol 113:73–86

Stebbins JF, Carmichael ISE, Moret LK (1984) Heat capacities and entropies of silicate liquids and glasses. Contrib Mineral Petrol 86:131–148

Thornber CR, Roeder PL, Foster JR (1980) The effect of composition on the ferric-ferrous ratio in basaltic liquids at atmospheric pressure. Geochim Cosmochim Acta 44:525–532

Thy P, Lofgren GE (1994) Experimental constraints on the low-pressure evolution of transitional and mildly alkalic basalts: the effect of Fe-Ti oxide minerals and the origin of basaltic andesites. Contrib Mineral Petrol 116:340–351

Toplis MJ, Carroll MR (1995) An experimental study of the influence of oxygen fugacity on Fe-Ti oxide stability, phase relations, and mineral-melt equilibria in ferro-basaltic systems. J Petrol 36:1137–1170

Virgo D (1987) The effect of oxidation state on the viscosity of melts in the system Na_2O-FeO-Fe_2O_3-SiO_2. Geochim Cosmochim Acta 51:195–205

Virgo D, Mysen BO (1985) The structural state of iron in oxidized vs. reduced glasses at 1 atm.: a ^{57}Fe Moessbauer study. Phys Chem Minerals 12:65–76

Virgo D, Mysen BO, Seifert FA (1981) Relationship between the oxidation state of iron and structure of silicate melts. Carnegie Inst Washington Year Book 80:308–311

Wallace P, Carmichael ISE (1992) Alkaline and calc-alkaline lavas near Los Volcanes, Jalisco, Mexico: geochemical diversity and its signficance in volcanic arcs. Contrib Mineral Petrol 111:423–439

Wallace P, Carmichael ISE (1994) Petrology of Volcan Tequila, Jalisco, Mexico: Disequilibrium phenocryst assemblages and evolution of the subvolcanic magma system. Contrib Mineral Petrol 117:345–361

Wilson AD (1955) A new method for the determination of ferrous iron in rocks and minerals. Bull Geol Surv Great Britain 9:56–58